

Three-dimensional conjugate gradient inversion of magnetotelluric sounding data*

Lin Changhong^{1,2}, Tan Handong^{1,2}, and Tong Tuo^{1,2}

Abstract: Based on the analysis of the conjugate gradient algorithm, we implement a three-dimensional (3D) conjugate gradient inversion algorithm with magnetotelluric impedance data. During the inversion process, the 3D conjugate gradient inversion algorithm doesn't need to compute and store the Jacobian matrix but directly updates the model from the computation of the Jacobian matrix. Requiring only one forward and four pseudo-forward modeling applications per frequency to produce the model update at each iteration, this algorithm efficiently reduces the computation of the inversion. From a trial inversion with synthetic magnetotelluric data, the validity and stability of the 3D conjugate gradient inversion algorithm is verified.

Keywords: magnetotelluric, 3D, inversion, conjugate gradient

Introduction

In recent years, 3D forward modeling and inversion have been hot topics in the field of electromagnetics. 3D inversion of magnetotelluric data requires higher computer hardware resources and more time for computation because of large amounts of data and many parameters. The key problem for the introduction of magnetotelluric inversion into common practice is how to rapidly and accurately obtain inversion results. Therefore, many geophysicists focus on research of the kinds of algorithms which can reduce compute time and enhance the efficiency of the process. 2D magnetotelluric inversion algorithms include nonlinear least-squares solutions (Jupp and Vozoff, 1977), conjugate gradients (Madden and Mackie, 1989), Occam's inversion (DeGroot-Hedlin and Constable, 1990), and rapid

relaxation (Smith and Booker, 1991). 3D inversion methods include restricted 3D inversion methods, such as maximum likelihood inversion using conjugate gradients (Mackie and Madden, 1993), nonlinear conjugate gradient inversion (Newman and Alumbaugh, 2000), artificial neural networks (Spichak and Popova, 2000), and approximate 3D inversion methods (Hu et al., 2006) like quasi-linear approximation (Zhdanov et al., 2000) and rapid relaxation (Tan et al., 2003b). Based on the theoretical comparison of two conjugate gradients methods (nonlinear conjugate gradient and Mackie-Madden) and the Gauss-Newton algorithm for efficiency using synthetic and field magnetotelluric data, Rodi and Mackie (2001) concluded that conjugate gradient method would be a much more feasible approach to 3D electromagnetic inversion.

In this paper, we introduce a 3D conjugate gradient inversion algorithm for magnetotelluric impedance

Manuscript received by the Editor September 20, 2008, revised manuscript received November 5, 2008.

*This work is jointly sponsored by National Natural Science Foundation of China (Grant Nos. 40774029, 40674037, and 40374024), the National Hi-tech Research and Development Program of China (863 Program) (No. 2007AA09Z310) and the Program for New Century Excellent Talents in University (NCET).

1. State Key Lab of Geological Processes and Mineral Resources, China University of Geosciences, Beijing, 100083, China.
2. School of Geophysics and Information Technology, China University of Geosciences, Beijing, 100083, China.

data. Forward modeling for computing the impedance response will be discussed first. Second, we will discuss the theory of the inversion, including the objective function, a flowchart of the inversion process, and the pseudo-forward problem (Rodi and Mackie, 2001). Finally, the results of 3D inversion with synthetic data will be shown.

The 3D Forward problem

The 3D forward problem needs to consider how to correctly simulate the model response arising from complex realistic 3D geology. The staggered-grid finite difference method (Tan et al., 2003a) can solve this problem well.

The magnetotelluric field satisfies the integral form of the Maxwell equations:

$$\oint \mathbf{H} \cdot d\mathbf{l} = \iint \mathbf{J} \cdot d\mathbf{S} = \iint \sigma \mathbf{E} \cdot d\mathbf{S}, \quad (1)$$

$$\oint \mathbf{E} \cdot d\mathbf{l} = \iint i\mu_0 \omega \mathbf{H} \cdot d\mathbf{S}. \quad (2)$$

With the discretization of the Maxwell equations with a staggered grid (figure 1), a linear system results:

$$\mathbf{KH} = \mathbf{s}. \quad (3)$$

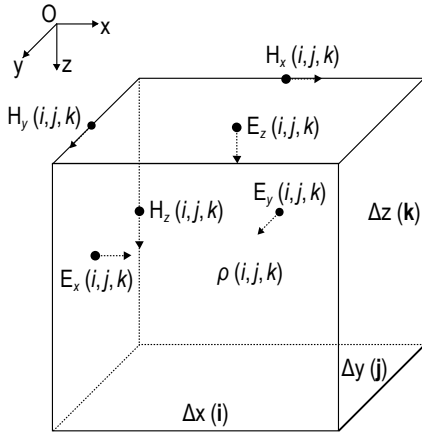


Fig. 1 The length, width, height, and resistivity of the staggered grid cell labeled by (i, j, k) are $\Delta x(i)$, $\Delta y(j)$, $\Delta z(k)$, and $\rho(i, j, k)$. The six components of the electric and magnetic fields in the cell are determined by the following principle: the magnetic fields are sampled in the middle of cell edges and the electric fields on the cell face centers. $H_x(i, j, k)$, $H_y(i, j, k)$, and $H_z(i, j, k)$ are defined as the mean value of the magnetic fields along cell edges and $E_x(i, j, k)$, $E_y(i, j, k)$, and $E_z(i, j, k)$ as the mean value of the electric fields along the cell faces.

\mathbf{K} is a complex-symmetric sparse matrix with at most 13 non-zero elements per row, \mathbf{H} is a vector composed of the three magnetic field components, and \mathbf{s} is the source vector related to the boundary conditions. The magnetic field \mathbf{H} will be obtained using the conjugate gradients method to solve equation (3). Then, the electric field \mathbf{E} will be obtained by the equation $\nabla \times \mathbf{H} = \sigma \mathbf{E}$. Finally, the impedance response of the 3D model can be found from equation (4) with \mathbf{H} and \mathbf{E} .

The magnetotelluric source \mathbf{S} can always be divided into two orthogonal sources, \mathbf{S}_X and \mathbf{S}_Y (Tan et al., 2004). Under the influence of \mathbf{S}_X , the component of the electric field, the component of the magnetic field, and the magnetic field can be denoted by E_{x1} , E_{y1} , H_{x1} , H_{y1} and H_1 . The corresponding value under the influence of \mathbf{S}_Y can be denoted by E_{x2} , E_{y2} , H_{x2} , H_{y2} and H_2 . Then, the expressions used to compute the impedance tensor are:

$$Z_{xx} = \frac{E_{x1}H_{y2} - E_{x2}H_{y1}}{H_{x1}H_{y2} - H_{x2}H_{y1}}, \quad (4a)$$

$$Z_{xy} = \frac{E_{x2}H_{x1} - E_{x1}H_{x2}}{H_{x1}H_{y2} - H_{x2}H_{y1}}, \quad (4b)$$

$$Z_{yx} = \frac{E_{y1}H_{y2} - E_{y2}H_{y1}}{H_{x1}H_{y2} - H_{x2}H_{y1}}, \quad (4c)$$

$$Z_{yy} = \frac{E_{y2}H_{x1} - E_{y1}H_{x2}}{H_{x1}H_{y2} - H_{x2}H_{y1}}. \quad (4d)$$

3D Inversion problem

If $F(m)$ is defined as the forward modeling function to calculate impedance vector \mathbf{Z} , the observed impedance vector \mathbf{Z}^{obs} , model vector \mathbf{m} , and error vector \mathbf{e} satisfy the equation:

$$\mathbf{Z}^{obs} = F(\mathbf{m}) + \mathbf{e}. \quad (5)$$

$\mathbf{Z}^{obs} = [Z^{obs1}, Z^{obs2}, \dots, Z^{obsN}]^T$ is a data vector where Z^{obsi} denotes the real or imaginary part of the impedance tensor for a particular observation site and frequency f and N is the total number of the impedance values. We have $\mathbf{m} = [m^1, m^2, \dots, m^M]$ where M is the number of model blocks and m^j is the logarithm of resistivity for a unique block ($\log \rho$).

The objective function

Based on the “regularized solution” method of Tikhonov and Arsenin (1977), the objective function can be defined as:

Three-dimensional conjugate gradient inversion

$$\psi(m) = (Z^{obs} - F(m))^T V^{-1} (Z^{obs} - F(m)) + \lambda(m_0 - m)^T L^T L(m_0 - m). \quad (6)$$

Where λ is the regularization parameter, V is the variance of error vector e , L is a simple second-difference Laplacian, and m_0 is the initial model. The objective function has constraints on both the data error and the model.

Flowchart of the inversion process

A simple flowchart for the 3D conjugate gradient iterative inversion is listed as:

- (1) Set $i=0, j=0$ and input the initial model
- (2) Set the reference model with updated model parameters: $m_{ref}=m_i$ or $m_{ref}=m_j$
- (3) Calculate data error $e=Z^{obs}-F(m_{ref})$
- (4) Calculate the gradient of the objective function

$$g_i = -2A(m_{ref})^T V^{-1} e + 2\lambda L^T L(m_0 - m_{ref})$$
- (5) Calculate the objective function

$$\psi_i = e^T V^{-1} e + \lambda(m_0 - m_{ref})^T L^T L(m_0 - m_{ref})$$
- (6) If line search convergence fails, then
 $\alpha_j = (\alpha_{j-1} + \alpha_{i-1})/2$. Update the model parameters $m_j = m_{i-1} + \alpha_j p_{i-1}$, $j=j+1$ and return to step (2).
- (7) $h_i = Cg_i$
- (8) $\beta_i = h_i^T (g_i - g_{i-1}) / h_{i-1}^T g_{i-1}$
- (9) Update the search direction $p_i = -h_i + \beta_i p_{i-1}$
- (10) $f = A(m_{ref})p_i$
- (11) Update the step

$$\alpha_i = -p_i^T g_i / 2(f^T V^{-1} f + \lambda p_i^T L^T L p_i)$$
- (12) Update the model parameters $m_i = m_{i-1} + \alpha_i p_i$
- (13) $i=i+1$ and return to step (2).

In step (4) $A(m_{ref})$ is the Jacobian matrix. In step (7), C is a pre-conditioner

$$C = (\mathcal{H} + \lambda L^T L)^{-1}. \quad (7)$$

I is a unit matrix and γ is a specified scalar. With the pre-conditioner and linear system $(\gamma_e I + \lambda L^T L)h_0 = g_0$, the initial search direction $P_0 = h_0$ will be obtained.

The pseudo-forward modeling problem

The main computations in the complete inversion process are: the forward modeling $F(m_{ref})$ in step (3), computing the gradient of the objective function $g_i = -2A(m_{ref})^T V^{-1} e + 2\lambda L^T L(m_0 - m_{ref})$ in step (4), and computing $f = A(m_{ref})p_i$ in step (10). If we take the normal forward modeling $F(m_{ref})$ out of consideration, the model update at each iteration will occur after evaluating the quantities $A(m_{ref})^T V^{-1} e$ and $A(m_{ref})p$. Our 3D conjugate

gradient inversion algorithm doesn't need computation of every Jacobian matrix element $A(m_{ref})$ to calculate $A(m_{ref})^T V^{-1} e$ and $A(m_{ref})p$, but it directly gets the $A(m_{ref})^T V^{-1} e$ and $A(m_{ref})p$ values from several pseudo-forward modeling applications.

Since impedance data is used in the inversion, $A(m_{ref})^T V^{-1} e$ can be expressed as:

$$A(m_{ref})^T V^{-1} e = \sum_{n=1}^N (\partial Z_n / \partial m_k)^T (V^{-1} e)_n, \quad k=1,2,\dots,M. \quad (8)$$

Following the ideas of Newman and Alumbaugh (2000), differentiating each impedance tensor element at the j th observation site $(\partial z_{xxj} / \partial m_k, \partial z_{xyj} / \partial m_k, \partial z_{yxj} / \partial m_k$ and $\partial z_{yyj} / \partial m_k)$ with respect to the k th model parameter m_k yields:

$$\begin{aligned} \partial Z_{xxj} / \partial m_k = & {}^1 g_{jxx}^T K^{-1} (\partial K / \partial m_k H_1) \\ & + {}^2 g_{jxx}^T K^{-1} (\partial K / \partial m_k H_2) + C_{jxx}, \end{aligned} \quad (9a)$$

$$\begin{aligned} \partial Z_{xyj} / \partial m_k = & {}^1 g_{jxy}^T K^{-1} (\partial K / \partial m_k H_1) \\ & + {}^2 g_{jxy}^T K^{-1} (\partial K / \partial m_k H_2) + C_{jxy}, \end{aligned} \quad (9b)$$

$$\begin{aligned} \partial Z_{yxj} / \partial m_k = & {}^1 g_{jyx}^T K^{-1} (\partial K / \partial m_k H_1) \\ & + {}^2 g_{jyx}^T K^{-1} (\partial K / \partial m_k H_2) + C_{jyx}, \end{aligned} \quad (9c)$$

$$\begin{aligned} \partial Z_{yyj} / \partial m_k = & {}^1 g_{jyy}^T K^{-1} (\partial K / \partial m_k H_1) \\ & + {}^2 g_{jyy}^T K^{-1} (\partial K / \partial m_k H_2) + C_{jyy}. \end{aligned} \quad (9d)$$

where

$$\begin{aligned} {}^1 g_{jxx}^T = & [(H_{x1} H_{y2} - H_{x2} H_{y1})(-H_{y2}^e g_{jx}^T + E_{x2}^h g_{jy}^T) \\ & + (E_{x1} H_{y2} - E_{x2} H_{y1})(-H_{x2}^h g_{jy}^T + H_{y2}^h g_{jx}^T)] \\ & / (H_{x1} H_{y2} - H_{x2} H_{y1})^2, \end{aligned} \quad (10a)$$

$$\begin{aligned} {}^2 g_{jxx}^T = & [(H_{x1} H_{y2} - H_{x2} H_{y1})(-E_{x1}^h g_{jy}^T + H_{y1}^e g_{jx}^T) \\ & + (E_{x1} H_{y2} - E_{x2} H_{y1})(-H_{y1}^h g_{jx}^T + H_{x1}^h g_{jy}^T)] \\ & / (H_{x1} H_{y2} - H_{x2} H_{y1})^2, \end{aligned} \quad (10b)$$

$$\begin{aligned} {}^1 g_{jxy}^T = & [(H_{x1} H_{y2} - H_{x2} H_{y1})(-E_{x2}^h g_{jx}^T + H_{x2}^e g_{jx}^T) \\ & + (E_{x2} H_{x1} - E_{x1} H_{x2})(-H_{x2}^h g_{jy}^T + H_{y2}^h g_{jx}^T)] \\ & / (H_{x1} H_{y2} - H_{x2} H_{y1})^2, \end{aligned} \quad (10c)$$

$$\begin{aligned} {}^2 g_{jxy}^T = & [(H_{x1} H_{y2} - H_{x2} H_{y1})(-H_{x1}^e g_{jx}^T + E_{x1}^h g_{jx}^T) \\ & + (E_{x2} H_{x1} - E_{x1} H_{x2})(-H_{y1}^h g_{jx}^T + H_{x1}^h g_{jy}^T)] \\ & / (H_{x1} H_{y2} - H_{x2} H_{y1})^2, \end{aligned} \quad (10d)$$

$$\begin{aligned} {}^1 g_{jyx}^T = & [(H_{x1} H_{y2} - H_{x2} H_{y1})(-H_{y2}^e g_{jy}^T + E_{y2}^h g_{jy}^T) \\ & + (E_{y1} H_{y2} - E_{y2} H_{y1})(-H_{x2}^h g_{jy}^T + H_{y2}^h g_{jx}^T)] \\ & / (H_{x1} H_{y2} - H_{x2} H_{y1})^2, \end{aligned} \quad (10e)$$

$${}^2g_{jyx}^T = \left[(H_{x1}H_{y2} - H_{x2}H_{y1})(-E_{y1}{}^hg_{jy}^T + H_{y1}{}^eg_{jx}^T) + (E_{y1}H_{y2} - E_{y2}H_{y1})(-H_{y1}{}^hg_{jx}^T + H_{x1}{}^hg_{jy}^T) \right] / (H_{x1}H_{y2} - H_{x2}H_{y1})^2, \quad (10f)$$

$${}^1g_{jyy}^T = \left[(H_{x1}H_{y2} - H_{x2}H_{y1})(-E_{y2}{}^hg_{jx}^T + H_{x2}{}^eg_{jy}^T) + (E_{y2}H_{x1} - E_{y1}H_{x2})(-H_{x2}{}^hg_{jy}^T + H_{y2}{}^hg_{jx}^T) \right] / (H_{x1}H_{y2} - H_{x2}H_{y1})^2, \quad (10g)$$

$${}^2g_{jyy}^T = \left[(H_{x1}H_{y2} - H_{x2}H_{y1})(-H_{x1}{}^eg_{jy}^T + E_{y1}{}^hg_{jx}^T) + (E_{y2}H_{x1} - E_{y1}H_{x2})(-H_{y1}{}^hg_{jx}^T + H_{x1}{}^hg_{jy}^T) \right] / (H_{x1}H_{y2} - H_{x2}H_{y1})^2, \quad (10h)$$

$$C_{jyx} = (H_{y2}\partial^eg_{jx}^T / \partial m_k H_1 - H_{y1}\partial^eg_{jx}^T / \partial m_k H_2) / (H_{x1}H_{y2} - H_{x2}H_{y1}), \quad (10i)$$

$$C_{jxy} = (H_{x1}\partial^eg_{jx}^T / \partial m_k H_2 - H_{x2}\partial^eg_{jx}^T / \partial m_k H_1) / (H_{x1}H_{y2} - H_{x2}H_{y1}), \quad (10j)$$

$$C_{jyx} = (H_{y2}\partial^eg_{jy}^T / \partial m_k H_1 - H_{y1}\partial^eg_{jy}^T / \partial m_k H_2) / (H_{x1}H_{y2} - H_{x2}H_{y1}), \quad (10k)$$

$$C_{jyy} = (H_{x1}\partial^eg_{jy}^T / \partial m_k H_2 - H_{x2}\partial^eg_{jy}^T / \partial m_k H_1) / (H_{x1}H_{y2} - H_{x2}H_{y1}). \quad (10l)$$

where ${}^hg_{jx}^T$ and ${}^hg_{jy}^T$ are interpolator vectors between the x and y components of the magnetic field (H_{jx} , H_{jy}) at the j th observation site and the vector H : $H_{jx} = {}^hg_{jx}^T H$ and $H_{jy} = {}^hg_{jy}^T H$. While ${}^eg_{jx}^T$ and ${}^eg_{jy}^T$ are interpolator vectors between the x and y components of the electric field (E_{jx} , E_{jy}) at the j th observation site and the vector H : $E_{jx} = {}^eg_{jx}^T H$ and $E_{jy} = {}^eg_{jy}^T H$.

Plugging equation (9) into equation (8), we get:

$$A(m_{ref})^T V^{-1}e = H_1^T \partial K / \partial m_k K^{-1} \sum_{n=1}^N {}^1g_n(V^{-1}e)_n + H_2^T \partial K / \partial m_k K^{-1} \sum_{n=1}^N {}^2g_n(V^{-1}e)_n + \sum_{n=1}^N (C_n)^T (V^{-1}e)_n. \quad (11)$$

where, 1g_n , 2g_n and C_n are determined by equation (10). For example, if Z_{xyj} is the n th data value, then ${}^1g_n^T = {}^1g_{jxy}^T$, ${}^2g_n^T = {}^2g_{jxy}^T$ and $C_n = C_{jxy}$.

$$\text{If we set } {}^1v = K^{-1} \sum_{n=1}^N {}^1g_n(V^{-1}e)_n$$

$$\text{and } {}^2v = K^{-1} \sum_{n=1}^N {}^2g_n(V^{-1}e)_n$$

then

$$K {}^1v = \sum_{n=1}^N {}^1g_n(V^{-1}e)_n, \quad (12)$$

$$K {}^2v = \sum_{n=1}^N {}^2g_n(V^{-1}e)_n, \quad (13)$$

$$A(m_{ref})^T V^{-1}e = H_1^T \partial K / \partial m_k {}^1v + H_2^T \partial K / \partial m_k {}^2v + \sum_{n=1}^N (C_n)^T (V^{-1}e)_n. \quad (14)$$

If we take 1v as the vector to be solved and $\sum_{n=1}^N {}^1g_n(V^{-1}e)_n$ as the vector on the right side of the equation, equation (12) is similar to the forward modeling equation (3). Therefore, we call equation (12) a pseudo-forward modeling equation. The value of 1v can be obtained by solving the pseudo-forward modeling problem one time. Similarly, the value of 2v can be acquired by solving equation (13). Finally, $A(m_{ref})^T V^{-1}e$ in equation (14) can be obtained with the values of 1v and 2v .

Similarly, $A(m_{ref})p$ can be computed by solving the pseudo-forward modeling problem two times.

The 3D conjugate gradient inversion algorithm needs one forward modeling and four pseudo-forward modeling applications per frequency to produce the model update at each iteration. The vectors H_1 and H_2 result from one forward modeling step for two polarizations. The four pseudo-forward modeling applications will result in $A(m_{ref})^T V^{-1}e$ and $A(m_{ref})p$. If the normal forward modeling is removed, our algorithm only needs four pseudo-forward modeling applications. The number of pseudo-forward modeling applications in traditional inversion algorithms is usually the number of model parameters (or data). Therefore, our algorithm is one of the higher efficiency inversion algorithms.

Synthetic example

Based on the theory and equations above, we have developed a procedure to realize the 3D conjugate gradient inversion algorithm. To verify the correctness of this algorithm, we designed some 3D geologic models. The impedance response was calculated by staggered-grid finite difference modeling. Two percent Gaussian random noise was added to the data. All results were computed on a PC with an Intel 3.4 GHz Pentium (R) D CPU with 2 GB of memory.

Model 1: a 3D rectangular prism

The 3D rectangular prism dimensions are 6 km × 6 km × 3 km (see figure. 2). The 10 Ω·m prism body

Three-dimensional conjugate gradient inversion

is embedded in a $100\Omega\cdot m$ background with the top 3km below the earth's surface. The 3D grid size is $38 \times 38 \times 25$. Z_{xy} and Z_{yx} data at four frequencies ($3.3 - 0.1\text{ Hz}$) were measured at 256 sites and used in the inversion. After 43 iterations (10 hours and 9 minutes), the Chi-square error was down to 1.12 and the computations were stopped (see figure. 2). The results shown in Fig. 3 reflects the distribution of the real model well. The comparison between input impedance data at 0.1 Hz and the impedance response of the model are shown in figure. 4. The input impedance data matches well with the impedance response of the model.

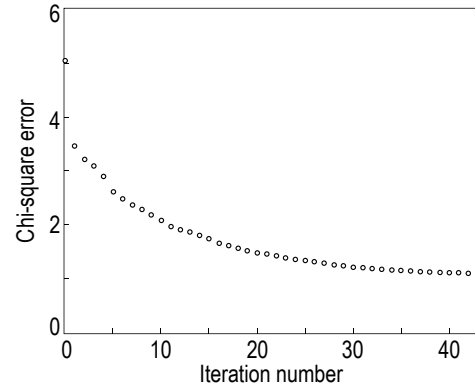


Fig. 2 The X axis is iteration number and the Y axis is chi-square error.

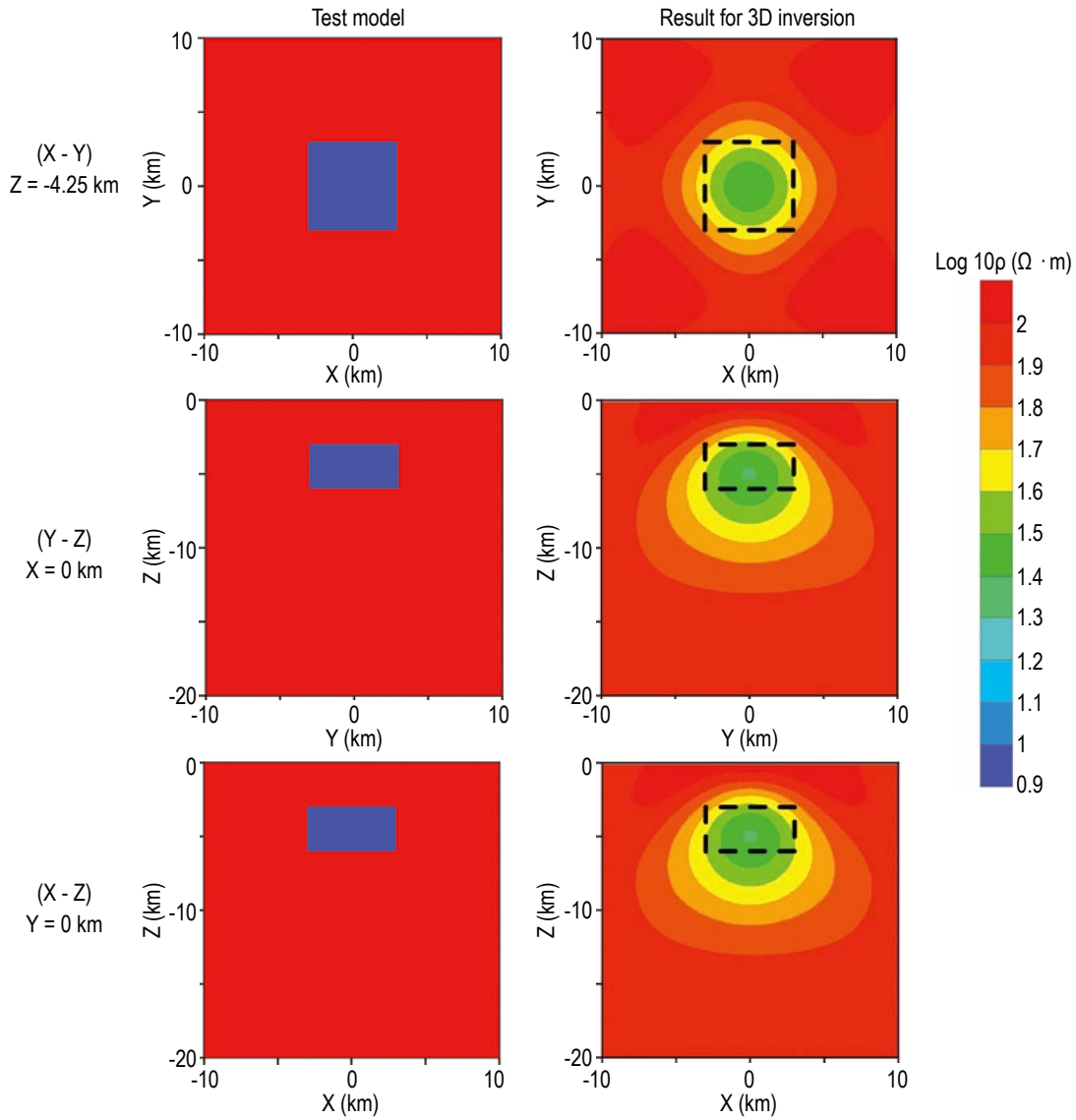


Fig. 3 The left side shows test model and the right side shows the result from the inversion. Black dotted lines shows the margin of prisms. The top row is the horizontal slice at 4.25 km depth, the middle row is the vertical slice along axis Y , and the bottom row is the vertical slice along axis X .

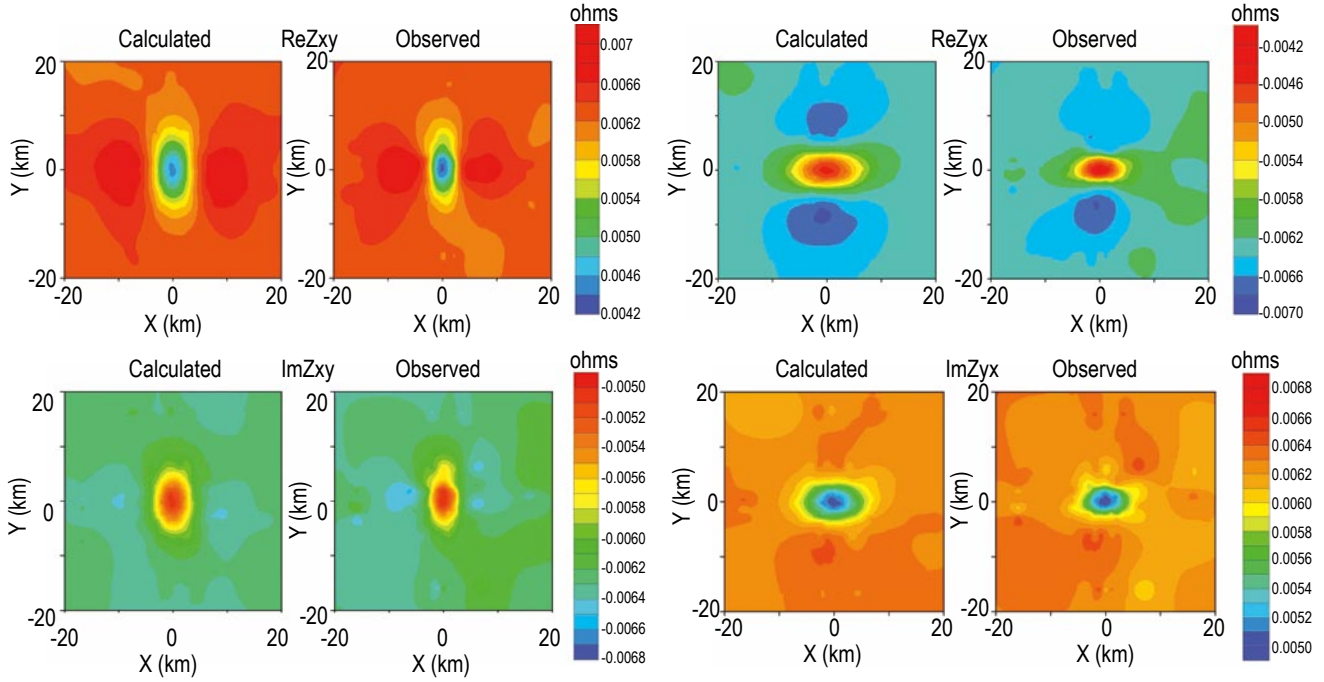


Fig. 4 The second and fourth columns (Observed) show input impedance data and the first and third columns (Calculated) show the impedance response of result model. ReZxy denotes the real part of Zxy and ReZyx denotes real part of Zyx; ImZxy denotes imaginary part of Zxy and ImZyx denotes imaginary part of Zyx.

Model 2: 3D rectangular prism with buried layer

The model is the same as in Model 1 except for the 1 km deep $50 \Omega \cdot m$ layer. The 3D grid size is $38 \times 38 \times 27$. Zxy and Zyx data at eight frequencies ($3.33 - 0.01$ Hz) were measured at 256 sites and used in the inversion. After 52 iterations (25 hours and 11 minutes), the Chi-square error was down to 1.15 and the computations were stopped (figure. 5). We see from figure. 6 that the reflection of the prism is comparably reproduced while the resistivity in the middle of the buried layer is a bit higher because of the influence of the prism. The comparison between input impedance data at 0.1 Hz and the impedance response of result model is shown in figure 7. The input impedance data match well with the impedance response of the model.

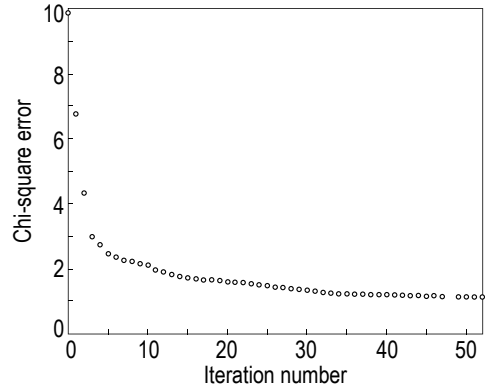
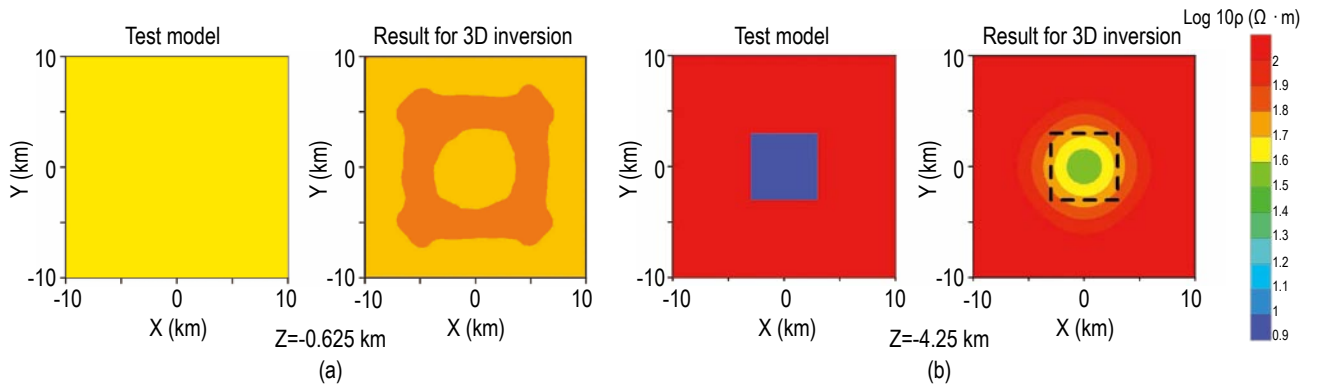


Fig. 5 The X axis is iterative number, the Y axis is chi-square error.



Three-dimensional conjugate gradient inversion

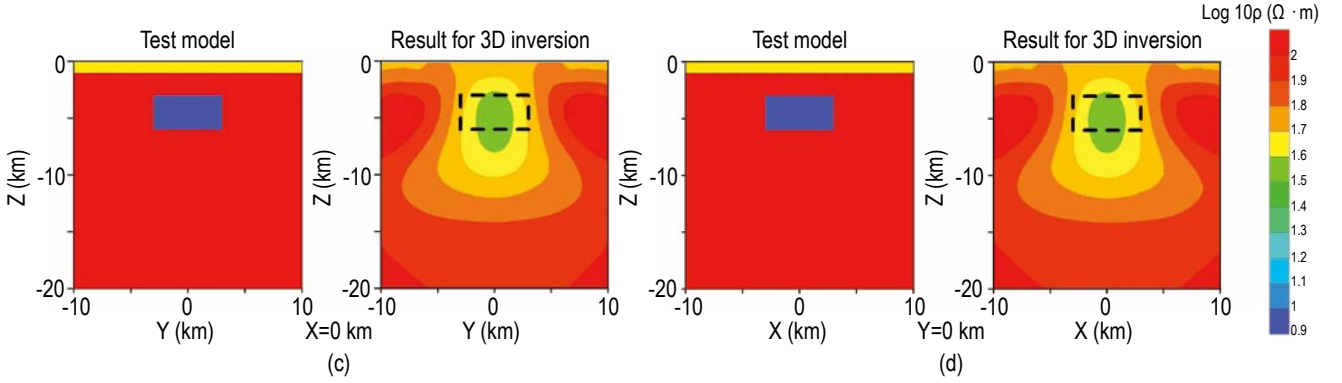


Fig. 6 The left panels of figures (a), (b), (c), and (d) show test models and the right panels of figures (a), (b), (c), and (d) show the results from inversion. The black dotted lines show the prism margins. The figure(a) is the horizontal slice at 0.625 km depth and the figure (b) is the horizontal slice at 4.25 km depth; The figure (c) is the vertical slice along Y axis and the figure (d) is the vertical slice along X axis.

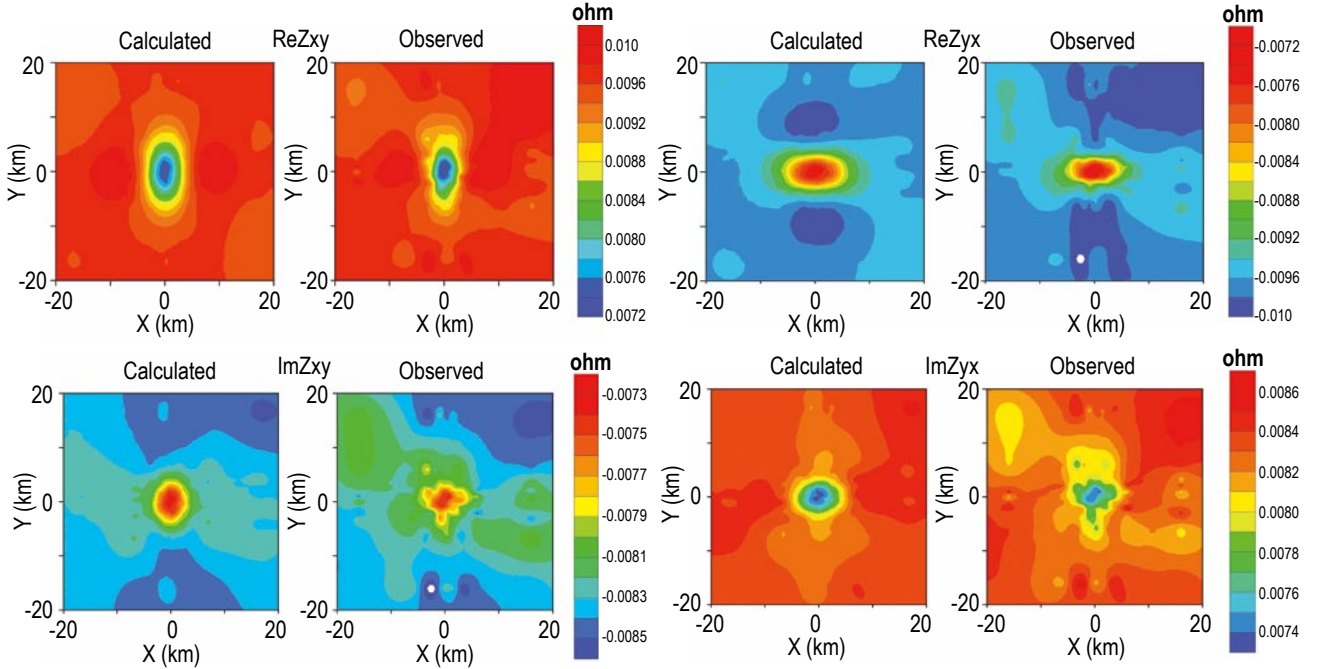


Fig. 7 The second and fourth columns (Observed) show input impedance data and the first and third columns (Calculated) show the impedance response of result model. ReZxy denotes the real part of Zxy and ReZyx denotes real part of Zyx; ImZxy denotes imaginary part of Zxy and ImZyx denotes imaginary part of Zyx.

Conclusions

We have developed a 3D conjugate gradient magnetotelluric inversion algorithm. During the inversion process, the algorithm doesn't need to compute and store the Jacobian matrix A but directly updates the model from the computation of the Jacobian matrix A and its transpose A^T multiplying the x vector. The Jacobian matrix A (or its transpose A^T) multiplying one x vector is equal to two pseudo-forward modeling applications. Therefore, this method needs only one forward modeling and four pseudo-forward modeling

applications at each iteration. In this way, it efficiently reduces the inversion computations. From the trial inversion with synthetic magnetotelluric data, our method has verified its feasibility.

In future work, we will research parallelizing the algorithm to further improve the efficiency of this method.

References

Avdeev, D. B., and Avdeeva, A. D., 2006, A rigorous three-

- dimensional magnetotelluric inversion: Progress in Electromagnetics Research, **62**, 41 – 48.
- DeGroot-Hedlin, C, and Constable, S., 1990, Occam's inversion to generate smooth, two-dimensional models from magnetotelluric data: Geophysics, **55**(12), 1613 – 1624.
- Hu, Z. Z., and Hu, X. Y., 2005, Review of three dimensional magnetotelluric inversion methods: Progress in Geophysics, **20**(1), 214 – 220.
- Hu, Z. Z., Hu, X. Y., and He, Z. X., 2006, Pseudo-three-dimensional magnetotelluric inversion using nonlinear conjugate gradients: Chinese Journal of Geophysics, **49** (4), 1226 – 1234.
- Jupp, D. L. B., and Vozoff, K., 1977, Two-dimensional magnetotelluric inversion: Geophys. J. Roy. Astr. Soc., **50**, 333 – 352.
- Madden, T. R., and Mackie, R. L., 1989, Three-dimensional magnetotelluric modeling and inversion: Proc. IEEE, **77**, 318 – 333.
- Mackie, R. L. and Madden, T. R., 1993, Three-dimensional magnetotelluric inversion using conjugate gradients: Geophys. J. Int., **115**, 215 – 229.
- Newman, G. A., and Alumbaugh, D. L., 2000, Three-dimensional magnetotelluric inversion using non-linear conjugate gradients: Geophys. J. Int., **140**, 410 – 424.
- Newman, G. A., and Boggs, P. T., 2004, Solution accelerators for large scale 3D electromagnetic inverse problems: 74th Ann. Internat. Mtg., Soc. Expl. Geophys., Expanded Abstracts, 680 – 683.
- Rodi, W., and Mackie, R. L., 2001, Nonlinear conjugate gradients algorithm for 2-D magnetotelluric inversion: Geophysics, **66**, 174 – 187.
- Spichak V., and Popova., 2000, Artificial neural network inversion of magnetotelluric data in terms of three-dimensional earth macroparameters: Geophys. J. Int., **142**, 15 – 26.
- Smith, J. T., and Booker, J. R., 1991, Rapid inversion of two- and three-dimensional magnetotelluric data: J. Geophys. Res., **96**, 3905 – 3922.
- Siripunvaraporn, W., Egbert, G., Lenbury, Y., and Uyeshima, M., 2005, Three-dimensional magnetotelluric inversion: data-space method: Physics of The Earth and Planetary Interiors, **150**(1 – 3), 3 – 14.
- Tan, H. D., Yu, Q. F., Booker, J., Wei, W., 2003a, Magnetotelluric three-dimensional modeling using the staggered-grid finite difference method: Chinese Journal of Geophysics, **46**(5), 705 – 711.
- Tan, H. D., Yu, Q. F., Booker, J., Wei, W., 2003b, Three-dimensional rapid relaxation inversion for the magnetotelluric method: Chinese Journal of Geophysics, **46**(6), 850 – 855.
- Tan, H. D., Wei, W., Deng, M., and Jin, S., 2004, General use formula in MT tensor impedance: Oil Geophysical Prospecting, **39**(1), 114 – 116.
- Tikhonov, A. N., and Arsenin, V. Y., 1977, Solutions of ill-posed problems: V. H. Winston and Sons.
- Wu, X. P., and Xu, G. M., 2000, Study on 3-d resistivity inversion using conjugate gradient method: Chinese Journal of Geophysics, **43**(3), 420 – 427.
- Zhdanov, M. S., Fang, S., and Hursan, G., 2000, Electromagnetic inversion using quasi-linear approximation: Geophysics, **65**(5), 1501 – 1513.
- Zhdanov, M., and Tolstaya, E., 2004, Minimum support nonlinear parametrization in the solution of a 3D magnetotelluric inverse problem: Inverse Problems, **20**(3), 937 – 952.

Lin Changhong graduated from the School of



Geophysics and Information Technology of China University of Geosciences (Beijing) with a Bachelor degree in 2001. Currently he is studying for his PhD at China University of Geosciences (Beijing).

位矢量, 本文导出了矢量波场弹性波 Kirchhoff 偏移方程。基于该方程, 利用炮记录同相轴斜率和射线追踪方法, 求得反射波的镜像反射点, 进而对反射数据进行 Fresnel 带偏移, 有效地降低了多波以非本波型速度传播造成的成像假像和有限孔径接收造成的偏移假象。模型试算表明了该方法的有效性和正确性。

关键词: Kirchhoff 偏移, 矢量波场, 纵波, 转换横波, 极化

河道砂体宽 / 窄方位三维观测系统地震物理模型分析 // A seismic modeling analysis of wide and narrow 3D observation systems for channel sand bodies, 狄帮让, 徐秀仓, 魏建新, **Applied Geophysics**, 5(4), P. 294-300.

(中国石油大学(北京)油气资源与探测国家重点实验室、CNPC 物探重点实验室 北京)

摘要:“宽 / 窄方位三维观测系统对地质目标地震成像分辨率的影响”是近年来 精度三维地震采集方法研究中的一个争论问题, 本文利用三维地震物理模拟技术的优势, 对上述争论问题进行实验研究。选择河道砂沉积构建地质模型, 设计宽方位(16 线)和窄方位(8 线)两种观测系统进行三维模拟数据采集和处理, 最后通过对三维偏移数据体的时间切片进行细致的宏观定性对比和微观定量分析, 得出如下结论: 在上覆地层相对平缓、速度横向变化不大的地质背景下, 三维采集无论采用宽方位还是窄方位, 都能对河道砂沉积实现高精度的地震成像, 并且两者的成像分辨率基本相当。

关键词: 地震物理模型, 地震成像, 宽 / 窄方位观测系统, 分辨率, 时间切片

地震低频伴影的数值模拟与应用 // Numerical simulation of seismic low-frequency shadows and its application, 贺振华, 熊晓军, 边立恩. **Applied Geophysics**, 5(4), P. 301 - 306.

(成都理工大学, 成都, 610059)

摘要: Taner 等人(1979)将油气储层正下方的地震低频强能量称为地震低频伴影, 并认为地震低频伴影可作为在地震记录上识别油气储层的标志之一。但产生低频伴影的物理机制到现在仍不清楚。为进一步探讨其机理, 论文作者采用了二维弥散-粘滞型波动方程对包含气层的地质模型进行地震数值模拟, 并在波场延拓过程中考虑了地震波的速度色散效应。对模拟地

震记录做时间-频率域的谱分析并抽取共频率剖面后, 发现了气层下方的地震低频强能量。模拟结果说明含气层对地震信号时频谱中高频成分的较强吸收衰减是产生低频伴影的主要原因。为地震低频伴影的解释与应用提供了依据。文中还给出了地震低频伴影的应用实例。该实例显示, 当地震资料具有较高信噪比时, 利用地震低频伴影可确定油气储层的存在及其空间分布范围。

关键词: 地震低频伴影, 数值模拟, 弥散-粘滞型波动方程, 速度色散, 油气储层识别

基于约束插值算法的井资料外推 // Extrapolate well logs based on the constrained interpolation algorithm, 刘红伟^{1,2}, 刘洪¹, 秦月霜³, 首皓⁴, **Applied Geophysics**, 5(4), P. 307 - 313.

(1. 中国科学院地质与地球物理研究所, 北京 100029; 2. 中国地质大学(北京)地质过程与矿产资源国家重点实验室, 北京 100083; 3. 中国石油大庆油田有限责任公司, 大庆 163712; 4. 中国石油勘探开发研究院, 北京 100083)

摘要: 本文在详细分析地震和测井方法属性差异的基础上, 系统讨论了声测井和地震资料的匹配问题, 提出了一种基于瞬时相位地层追踪的井震匹配方法。通过同相轴拉平技术使地震资料和井旁道资料同相位对比, 运用 SVD 方法求解方程得到插值系数, 并利用插值系数把测井资料外推, 从而得到同相轴连续, 分辨率高, 同时在井孔与测井资料能够匹配的地震资料。本方法应用于大庆 ma02 井区数据, 得到了很好的效果。

关键词: 同相轴拉平, SVD 方法, 瞬时相位

大地电磁法三维共轭梯度反演研究 // Three-dimensional Conjugate Gradients Inversion of Magnetotelluric Sounding data, 林昌洪, 谭捍东, 佟拓, **Applied Geophysics**, 5(4), P. 314 - 321.

(中国地质大学(北京)地球物理与信息技术学院, 北京, 100083)

摘要: 在对共轭梯度算法深入分析的基础上, 我们实现了大地电磁阻抗资料三维共轭梯度反演算法。三维共轭梯度反演算法的特点是反演过程中不需要实际计算和存储雅可比矩阵, 只需要计算雅可比矩阵的转置与一个向量的乘积以及雅可比矩阵与另一个向量的乘积, 直接可以得到模型修正量。三维共轭梯度反演算法每进行一次模型参数更新迭代只需要 1 次正演和 4 次“拟

正演”，有效的减少了反演的计算量。通过对理论模型合成数据进行反演试算，验证了所实现的大地电磁三维共轭梯度反演算法的有效性和稳定性。

关键词：大地电磁，三维，反演，共轭梯度

基于水文-地球物理模型的地下水污染磁电阻率异常动态监测仿真 // Time-dependent Magnetometric Resistivity Anomalies of Groundwater Contamination: Synthetic Results from Computational Hydro-geophysical Modeling, 朱凯光¹, 杨建文^{2,3}, **Applied Geophysics**, 5(4), P. 322 - 330.

(1. 吉林大学仪器科学与电气工程学院, 长春, 吉林, 130026, 中国; 2. 桂林工学院资源与环境工程系, 桂林, 广西, 541004; 3. 温莎大学地球与环境科学系, 温莎, 安大略, , N9B 3P4, 加拿大)

摘要：本文计算了地面磁电阻率法在监测地下水体中垃圾渗滤液运移的动态磁电阻率异常。基于对垃圾场地概念模型的水文地质仿真，建立了数值地电模型，并采用改进的有限差分软件MMR2DFD，分别计算了点源，MMR-TE方式，MMR-TM方式下半空间模型以及断层模型的磁电阻率异常响应。半空间模型的正演结果表明，垂直于主要电流方向的磁场分量包含更多地下异常信息，MMR-TE模式能有效进行地下水污染监测。断层模型的计算结果更进一步验证了MMR在地下水污染物运移监测中的有效性。

关键词：动态，磁电阻率，羽状渗滤液，水文地球物理模拟

10. 双层界面重磁联合反演方法研究 // Study of joint inversion of gravity and magnetic data for two-layer model, 江凡, 吴健生, 王家林, **Applied Geophysics**, 5(4), P. 331 - 339.

(同济大学海洋地质国家重点实验室, 上海 200092)

摘要：在Pilkington单层界面重磁同步联合反演工作的基础上，结合新一轮油气勘探对揭示新生界基底和结晶基底界面深度的需要，抓住中间层厚度、中心位置的变化与异常的关系提出了双层界面的重磁联合反演方法，通过理论模型的试验和实际例子的应用，说明了方法的有效性，也讨论了关键参数对算法的影响。

关键词：双层界面 重磁联合反演 新生界基底和结晶基底

生产油井井下温度场数值模拟分析 // Numerical simulation of downhole temperature distribution in producing oil wells, 石颖^{1, 2}, 宋延杰¹, 刘洪², **Applied Geophysics**, 5(4), P. 340 - 349.

(1. 大庆石油学院地球科学学院, 黑龙江 大庆 163318; 2. 中国科学院地质与地球物理研究所, 北京 100029)

摘要：针对大多数生产井多层产液的实际情况，本文提出了一种新的计算生产油井井下温度分布的加数值模拟方法，基于流体力学和热传递理论，建立了生产油井井下温度场在柱坐标系下的二维温度场模型。该模型考虑了热传导和由于流体在地层和井眼中流动引起的对流换热，同时还考虑了由多个产层生产引起的井筒中流体速度的变化。本文构建了井筒与围岩、井筒与产层、围岩与产层之间的耦合边界条件，采用交替方向半隐式(ADI)有限差分方法求解井下温度场模型，对比用此方法计算的理论模拟曲线与实测温度曲线，计算结果与实测结果接近。理论模拟结果表明，产液量、生产时间、孔隙度、层厚以及地温梯度对井下温度分布均有影响。

关键词：油井，井下温度场，热传递，数值模拟